# Effects of osmotic force and torque on microtubule bundling and pattern formation

Yongxing Guo,[1] Yifeng Liu,[1] Rudolf Oldenbourg,[2] Jay X. Tang,[1] and James M. Valles, Jr.[1]

[1]*Department of Physics, Brown University, Providence, Rhode Island 02912, USA*

[2]*Marine Biological Laboratory, Woods Hole, Massachusetts 02543, USA*

We report effects of polyethylene glycol (PEG, molecular weight of 35 kDa) on microtubule (MT) bundling and pattern formation. Without PEG, polymerizing tubulin solutions of a few mg/ml that are initially subjected to a field that aligns MTs can spontaneously form striated birefringence patterns. These patterns form through MT alignment, bundling, and coordinated bundle buckling. With increasing PEG concentrations, solutions form progressively weaker patterns. At a sufficiently high PEG concentration ($\sim$0.5% by weight), the samples maintain a nearly uniform birefringence (i.e., no pattern) and laterally contract at a later stage. Concomitantly, on a microscopic level, the network of dispersed MTs that accompany the bundles in pure solutions disappear and the bundles become more distinct. We attribute the weakening of the pattern to the loss of the dispersed MT network, which is required to mediate the coordination of bundle buckling. We propose that the loss of the dispersed network and the enhanced bundling result from PEG associated osmotic forces that drive MTs together and osmotic torques that facilitate their bundling. Similarly, we attribute the lateral contraction of the samples to osmotic torques that tend to align crossing bundles in the network.

## I. INTRODUCTION

Large macromolecules such as polymers, proteins, and nucleotides collectively occupy as much as 40% of the total volume of biological cells [1]. This macromolecular crowding can significantly alter the biochemical and biophysical properties of constituent molecules and can substantially alter their biomolecular functions [2]. In particular, large molecules or rodlike particles in a background of inert molecules experience osmotic forces and torques that can affect their self-assembly. The aggregation and alignment of rodlike particles are favorable because it tends to increase the volume available to the background molecules and thus, the entropy of the system [3]. Previous studies have shown that DNA [4], actin [5,6], and microtubules [7,8] more readily form bundles in the presence of inert macromolecules. Here we investigate how macromolecular crowding influences the structure of a microtubule assembly.

Microtubules (MTs), a major component of the eukaryotic cytoskeleton, must polymerize and form important structures within cells despite the crowded environment. Individual MTs play an integral role in intracellular transport in eukaryotes [9]. Structures consisting of multiple MTs such as the spindles and asters that are essential for mitosis [10] and parallel arrays and stripes that are necessary for directing early processes in embryogenesis [11,12] also appear. Many *in vitro* studies of MT organization have elucidated the mechanisms underlying their formation [13,14].

Recently, macroscopic patterns that appear in polymerizing purified tubulin solutions that contain neither motor proteins nor MT associated proteins [15,16] have drawn a great deal of attention. These patterns take the form of stripes, a few hundred microns wide, of varying MT orientation and density. In preceding work [17], we showed that the underlying microscopic structure initially consists of MTs that have been partially aligned by an external field. About one-half of these MTs form long parallel bundles that traverse

large domains of the sample ($\sim$mm). The other one-half form a dispersed elastic network. Over time, the bundles elongate as their constituent MTs continue to polymerize. They eventually buckle in coordination and nest with their neighbors to give rise to the wavelike array responsible for the macroscopic pattern. Although it is unclear whether these patterns serve any biological function, the physical processes involved in creating them undoubtedly can occur in cells.

Calculations suggest [18] that the dispersed network of MTs also plays an essential role in this pattern formation process. First, the network exerts a transverse restoring force that promotes buckling with a wavelength substantially shorter than the sample size. Without the transverse restoring force, only Euler buckling could occur and the wavelength would exceed the sample size. Second, the network provides the elastic coupling necessary for the bundles to buckle in coordination. This coordination reduces the critical buckling stress to the point that it can be generated by the polymerization of MTs within the bundles.

This microscopic picture of the generation of the stripe pattern suggests that the process would be susceptible to macromolecular crowding, which acts to promote lateral aggregation. Consequently, we have investigated the effects of adding polyethylene glycol (PEG), an inert polymer, to polymerizing concentrated tubulin solutions to test our model of the process and the robustness of this pattern formation mechanism. This approach is similar to that employed by others in investigations of various other biomolecular processes ranging from protein filament assembly [19], ion channel opening and closing [20], to transcription of DNA [21]. It differs, however, from the use of a porous matrix, which provides static crowding that reduces diffusion and confines polymeric growth [22]. We show how the introduction of PEG alters this macroscopic pattern and the underlying processes responsible for it. We observe dramatic changes that suggest that macromolecular crowding can exert a strong influence on the development of MT networks in cells and other physiological settings.

## II. MATERIALS AND METHODS

### A. Sample preparation

Tubulin was isolated from bovine brain by two cycles of assembly and disassembly followed by chromatography on phosphor cellulose [23]. It was then polymerized in 1 M glutamate sodium salt following an established protocol [24]. After centrifugation at 35 °C, MT pellets were homogenized and resuspended in PM buffer (100 mM PIPES, 1 mM EGTA, 2 mM $MgSO_4$, 0.5 mM GTP, $p$H 6.9), frozen in 200 $\mu$l aliquots and stored at −80 °C. We examined the purity of the tubulin preparation by Commassie Blue staining of proteins loaded (50 $\mu$g per lane) and separated on SDS-PAGE mini-gels, which showed no visible band other than that of tubulin. Immediately prior to use, tubulin solutions were thawed and then centrifuged at 1800 g for 5 min at 4 °C to remove small amounts of aggregates. For all our samples, the GTP concentration was 2 mM. Samples were degassed (after the addition of GTP) in cuvettes at 4 °C to prevent the air bubble formation that would otherwise occur during the increase in temperature to 37 °C. The cuvettes were then incubated on ice for 10 mins prior to inducing polymerization. The rectangular cuvettes have dimensions $40 \times 10 \times 1$ mm quartz (International Crystals, Oklahoma City, OK) or $50 \times 8 \times 0.4$ mm glass (Vitrocom, New Bedford, MA).

The radius of gyration $R_g$ for the 35 kDa PEG used in these studies is 11.4 nm [5], which is comparable to the radius of MTs: $R_M \approx 12$ nm. The w/w concentration of PEG ($C_{PEG}$) was varied from 0.05% to 1.0%. The concentration beyond which PEG molecules start to overlap is about 0.9% [5]. PEG was added to the tubulin solution at 4 °C before polymerization.

### B. Alignment of MTs using static magnetic fields

The application of static magnetic fields is recognized to be a nonintrusive mechanical method to align biological samples [25–31]. In particular, the alignment of MTs in a magnetic field of a few Tesla has been shown by Bras *et al.* [27]. Theoretical estimation shows that the minimum field strength needed to align a 5 $\mu$m MT parallel to the magnetic field direction is about 7.6 Tesla [27]. For MTs longer than 5 $\mu$m, the required field strength is even smaller. The magnetic field in our experiments was produced by a superconducting magnet system (American Magnetics, Oak Ridge, TN) with a room temperature bore. The diameter of the bore is 11 mm. Precooled tubulin solutions in glass cuvettes were placed in a 9 Tesla vertical magnetic field oriented parallel to the long axis of the cuvettes. The temperature of the bore was pre-equilibrated to 37 °C by circulating warm air through it from above. The sample temperature rose from 0 °C to 37 °C in about 100 s. Therefore, MT assembly was initiated by the temperature rise while in the presence of magnetic field. Observations and measurements were made at either room temperature or 30 °C, when specified, after the sample was removed from the magnet.

### C. Imaging birefringence patterns

Microtubules and aligned assemblies of microtubules can be imaged using polarized light techniques. Their inherent optical anisotropy causes light polarized parallel to their axis of alignment to travel more slowly than light polarized perpendicular to it. In general, this "birefringence" is characterized by the difference in the indices of refraction along these two perpendicular directions and the orientation of the axis of slower light propagation or the "slow axis." Images of the birefringence of tubulin samples were obtained by placing them between sheets of polarizing film (Edmund Optics, Blackwood, NJ) oriented with their axes of transmission at 90° (extinction 99.98%) and illuminating them with a light box (Hall Productions, Grover Beach, CA). Eight-bit depth images were recorded by a charge-coupled device camera (XCD-SX900; Sony) driven by FIRE-I software at a resolution of $1280 \times 1024$. The long axis of the cuvette was set at either 45° or 0° with respect to the polarization directions of the polarizers. Bright regions of the images correspond to regions in which MTs are not parallel to either of the polarizer directions.

### D. Quantitative birefringence and fluorescence microscopy

The birefringence of MT patterns and bundles was measured using a polarizing microscope that was equipped with a liquid crystal universal compensator (LC-PolScope, Cambridge Research and Instrumentation, Woburn, MA) and operated as described in [32,33]. LC-PolScope software was used for instrument control and image capture. It was also employed for the pixel-by-pixel computation of sample retardance, which is equal to the index of refraction difference referred to above multiplied by the sample thickness and slow axis orientation maps. For further analysis, images were transferred to ImageJ, a public domain image processing and analysis software (Rasband, ImageJ, U. S. National Institutes of Health, Bethesda, MD).

Fluorescence measurements were performed with a Nikon TE800 microscope and a Photometrics Cool-Snap HQ high-resolution camera bundled with the MetaMorph software (Molecular Devices Inc., Downingtown, PA). MTs were labeled with Oregon green-conjugated taxol (taxol-Oregon green) (Molecular Probes, Eugene, OR). Blue light (peak wavelength 480 nm) was used for excitation, and the green light emitted by the taxol-Oregon green (peak wavelength 532 nm) was measured.

## III. RESULTS

### A. Contraction effect caused by PEG

Without PEG, striated MT birefringence patterns form in tubulin solutions that are initially subjected to a 9 T magnetic field for the first 5 min of polymerization [34]. The static magnetic field is applied parallel to the long axis of the cuvette. At early times, the retardance of the samples is uniform [Figs. 1(a) and 1(c)]. The fact that the image is brighter for the 45° polarization configuration indicates that the MTs tend to align along the initial magnetic field direction. The birefringent stripes that form over the course of minutes to hours are perpendicular to the initial magnetic field direction [Figs. 1(b) and 1(d)]. With 0.5% PEG added to the tubulin solution, the MTs can still be aligned by the magnetic field,
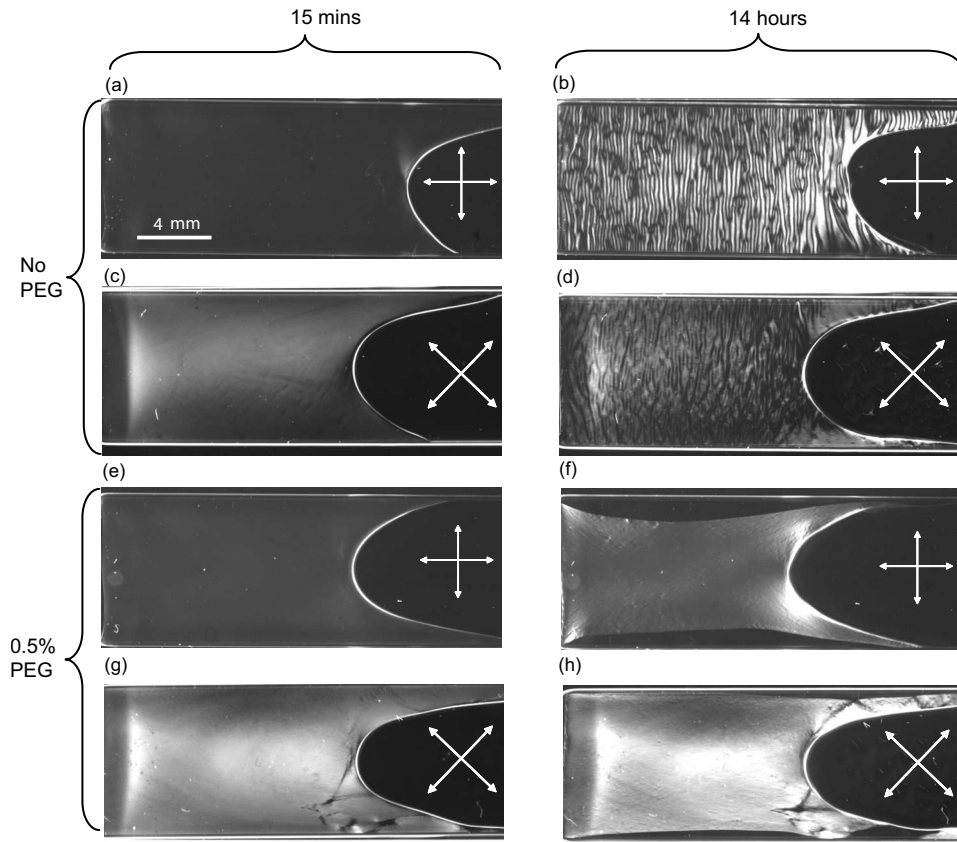
FIG. 1. MT birefringence pattern images [34] between crossed polarizers. Images on each row recorded at two different times are from the same sample; for example, the first row represents images from sample 1 and the second row is for sample 2. Samples 1 and 3 were recorded side by side; likewise for samples 2 and 4. The white crossed arrows indicate the directions of the crossed polarizers, at configurations either 0° or 45° relative to the long axis of each of the cuvettes. Note the detachment of the MT network from the wall in (f) and (h). The area of the sample containing the MT network decreased by about 30% from (e) to (f). The bright spot near the bottom center of the cuvettes in (c,d,g,h) is an artifact due to some built-in birefringence of the cuvettes, most noticeable when their long axis is 45° from the orientation of the polarizers. The average light intensities in the central sample regions in arbitrary units are, from (a) to (h), 26, 92, 103, 62, 42, 47, 143, and 166, all after background subtraction (65 for 0° configurations and 43 for 45° configurations).

as shown in Figs. 1(e) and 1(g), but the striated pattern does not subsequently form [Figs. 1(f) and 1(h)]. Instead, the samples exhibit a nearly uniform retardance and an interesting contraction effect. The contraction leaves regions devoid of MTs. Specifically, the area occupied by the MT network decreases by as much as 30% as shown by Figs. 1(e) and 1(f). This contraction appears anisotropic in the plane of observation, being largest in the direction perpendicular to the initial magnetic field.

### B. Suppression of coordinated buckling

The suppression of the pattern by the introduction of PEG is evident in fluorescence images [Figs. 2(b) and 2(c)]. Without PEG, static undulations in the fluorescence intensity are visible while the intensity is uniform across samples with large $C_{PEG}$. Since the intensity is proportional to the MT density, the static undulations reflect its spatial variations. The spatially averaged intensities in the two images are the same within our experimental resolution, indicating that the total number of MTs polymerized does not depend on PEG concentration.

Our quantitative retardance measurements indicate that the pattern suppression occurs gradually with increasing PEG concentration, $C_{PEG}$. Figure 3, which shows images of the retardance and slow axis orientations of three samples with $C_{PEG}$ of 0.05%, 0.1%, and 0.5% demonstrates this phenomenon. To quantify this suppression, the slow axis orientation along the central line of the cuvette was fitted to $\varphi(x) = \arctan\{A\frac{2\pi}{\lambda}\cos[\frac{2\pi}{\lambda}(x+x_0)]\}$ [18] (white curves in Fig. 3). From the fitted curves, the buckling wavelength and amplitude can be obtained. The buckling wavelength is about 500 $\mu$m for $C_{PEG}$ of 0.05% and 0.1%. This value is comparable to that observed in our previous studies on samples without PEG [17,18] and it is much larger than the buckling wavelength of a single MT in a living cell [35]. The buckling amplitude decreases by about 50% from $A=57$ $\mu$m for the 0.05% sample to $A=28$ $\mu$m for the 0.1% sample. When the $C_{PEG}$ is increased to 0.5%, no obvious static undulations are apparent, indicating that the buckling of the MT bundles is totally suppressed [Fig. 3(c)]. Interestingly, the retardance average over this sample is about 2 times as large as that in the two samples exhibiting static undulations. This difference, taken with the indication from the fluorescence imaging that the averaged density of MTs does not depend on
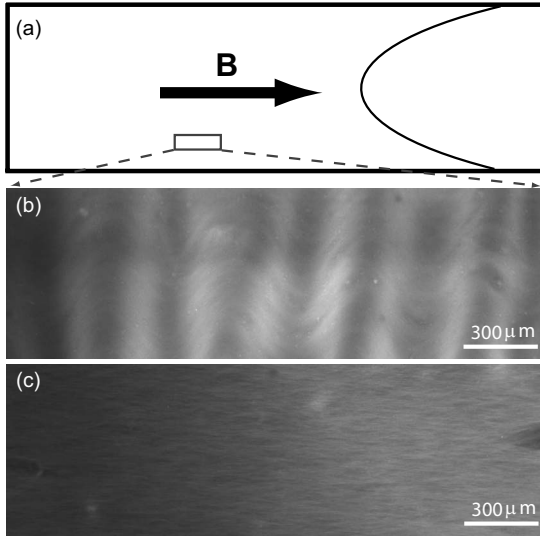
FIG. 2. (a) Schematic drawing of the cuvette in a 9 T magnetic field during the first 5 minutes of polymerization. The small gray rectangle indicates the region where the fluorescence images in (b) and (c) were taken [34]. (b) Fluorescence image of a sample without PEG. (c) Fluorescence image of a sample with 0.5% w/w PEG. Both images were taken at about 12.5 h after initialization of polymerization. The average fluorescence intensities of the two images are the same within experimental error.

PEG concentration, suggests that PEG enhances the local alignment of MTs.

### C. PEG induced clearing of dispersed MTs

To investigate the influence of PEG on the microscopic structure of the MT samples, we polymerized a series of samples with different PEG concentrations and examined them with high resolution fluoresence microscopy. The samples were polymerized in Eppendorf tubes so that we could easily extract material for the slide preparations. The fluorescence images reveal that the vast majority of MTs become incorporated into MT bundles at high $C_{PEG}$. For $C_{PEG}=0$ [Fig. 4(a)], the MTs form "fuzzy" bundles immersed in a dispersed network of MTs. For $C_{PEG}=0.05\%$ [Fig. 4(b)], there are fewer MTs in the dispersed network and the bundles become more clearly defined. At the highest concentration, for $C_{PEG}=0.1\%$ [Fig. 4(c)], the dispersed network has all but disappeared and the bundles appear thick and well defined. Moreover, many of these bundles develop discernible ends.

### D. MT bundle size distribution

Because the MT bundles become so distinct at high $C_{PEG}$, it becomes possible to measure their size distribution. Previous studies show that the integrated retardance of a MT bundle is proportional to the number of MTs in its cross section and that the integrated retardance of a single MT is determined as $A=7.5$ nm$^2$ [33,36]. Figure 5(a) shows a retardance image of MT bundles formed in a solution with 1% w/w PEG and 3.6 mg/ml tubulin [37]. A line scan across
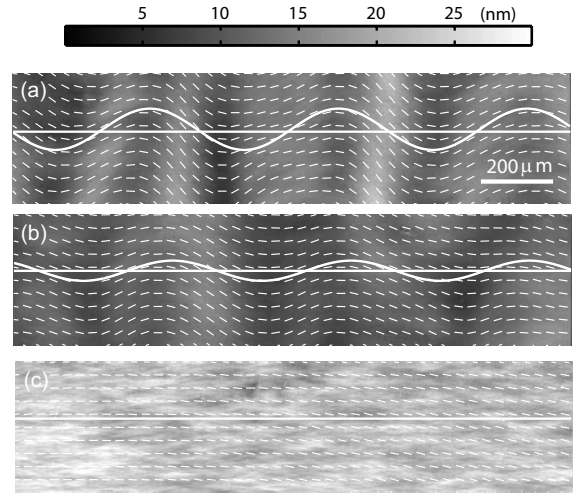


FIG. 3. Retardance images showing the amplitude of the buckling decreasing with increased $C_{PEG}$. These retardance images of three samples [34] with 0.05% (a), 0.1% (b), and 0.5% (c) w/w PEG, respectively, were obtained using an LC-PolScope imaging system. The grey scale bar on the top shows the retardance magnitude and the white pins illustrate the slow axis orientation. The straight white lines represent the line scan location for data analysis detailed previously [18]. The slow axis orientation line scan data were fitted to $\varphi(x)=\arctan\{A\frac{2\pi}{\lambda}\cos[\frac{2\pi}{\lambda}(x+x_0)]\}$ and the white curve is the sinusoidal function of the MT bundle contour with wavelength $\lambda$ and amplitude $A$. (a) Image of a sample with 0.05% w/w PEG, taken at about 18 hours after initialization of polymerization. $\lambda\approx522$ $\mu$m, $A\approx57$ $\mu$m. The average retardance is $\bar{\Delta}\approx13.3$ nm. The standard deviation of the retardance line scan data is about 3.0 nm or 23.5% over the mean. (b) Image of a sample with 0.1% w/w PEG, taken at about 18 h after initialization of polymerization. $\lambda\approx494$ $\mu$m, $A\approx28$ $\mu$m. The average retardance is $\bar{\Delta}\approx11.3$ nm. The standard deviation of the retardance line scan data is about 2.2 nm or 19.5% over the mean. (c) Image of a sample with 0.5% w/w PEG, taken at about 14 h after initialization of polymerization. There is no observed buckling. The average retardance is $\bar{\Delta}\approx22.5$ nm. The standard deviation of the retardance line scan data is about 3.6 nm or 12.1% over the mean.

bundle number 4 yields the retardance cross section shown in Fig. 5(b) as a typical example. Integration of the scan gives 158.1 nm$^2$ and thus, bundle number 4 consists of about 21 MTs. The size distribution of 124 MT bundles is shown in Fig. 5(c). The average number of MTs in a bundle is around 41, which is comparable to the width of the distribution in the histogram, suggesting a wide range of spread in size. We found that the shapes of these distributions in samples with 0.5% and 1% PEG were similar to within random error. This similarity suggests that the size distribution does not change above 0.5% PEG.

### IV. DISCUSSION

The experimental results show that the addition of PEG substantially alters the macroscopic and microscopic evolution of polymerizing tubulin solutions. Our previous studies suggested that two populations of MTs form in samples with-
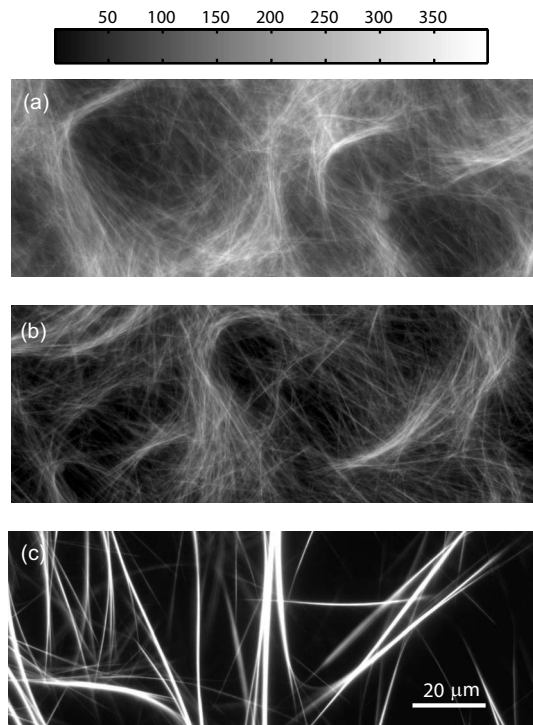
FIG. 4. Clearing of dispersed MTs and formation of discrete MT bundles induced by PEG. Fluorescence images of MT networks [37] polymerized from 3.6 mg/ml tubulin solutions in Eppendorf tubes without an applied magnetic field. The PEG concentrations were (a) 0%, (b) 0.05%, and (c) 0.1% by weight. The bar on the top shows the fluorescence intensity in gray scale. All the samples were labeled with 2 $\mu$M Oregon green conjugated taxol and the images were taken approximately 30 min after initialization of polymerization.

out PEG [17]. The first population consists of parallel, long MT bundles aligned along the magnetic field direction; the second consists of randomly oriented MTs that form an elastic network. It has been shown in our previous work [18] that the subsequent elongation of the MT bundles and their coordinated buckling produces the striated birefringence pattern. We concluded that the elastic, dispersed MT network surrounding the continuous, long MT bundles is required for the coordinated buckling to occur. Our results in this study indicate that the addition of PEG makes the bundles more distinct and drives individual MTs into bundles, eliminating the dispersed network. At the highest PEG concentrations, these samples develop nearly uniform birefringence and contract laterally.

Below, we attribute these microscopic and macroscopic changes to the influence on the MTs of osmotic forces and torques associated with the PEG. We estimate the osmotic forces and torques and show that they dominate the MT-MT interactions. We discuss how they lead to the microscopic morphology and how this morphology leads to the macroscopic evolution of the samples. Throughout, we presume that the PEG exerts a negligible influence on the MT polymerization kinetics and critical tubulin concentration since experiments have shown that such effects become apparent only at PEG concentrations that are an order of magnitude larger than those we have employed [38].
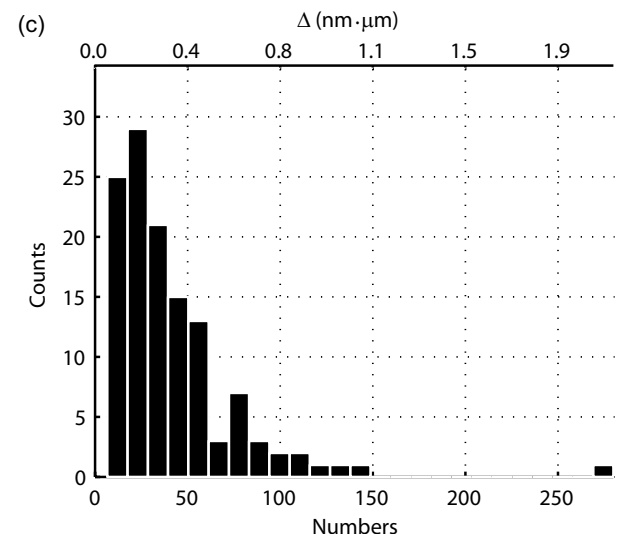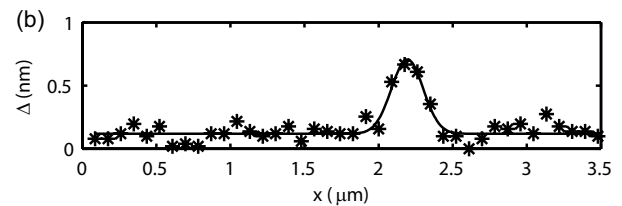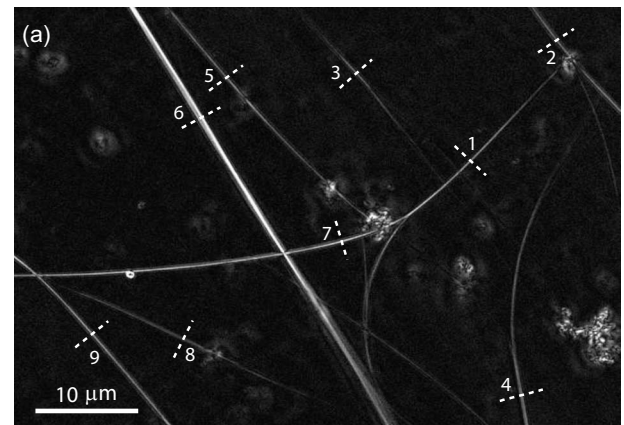


FIG. 5. MT bundle size distribution induced by 1% w/w PEG when polymerized from 3.6 mg/ml tubulin solution [37]. (a) Retardance image of MT bundles. The white dashed lines indicate the retardance line scan positions. The directions of these white dashed lines were determined by a customized Matlab program to be perpendicular to the MT bundle contours. (b) A typical line scan plot of the retardance data (stars; for bundle number 4), fitted to a Gaussian function (black curve). (c) Histogram of the size distribution of MT bundles. The top axis is the value of the integration of the fitted retardance curve from the retardance line scan data. The bottom axis shows the converted numbers of MTs at the cross sections of MT bundles. The average number of MTs at the cross section of a bundle is determined to be around 41, with a wide range of spread in size distribution.

### A. Binding energy between MTs due to osmotic pressure

In the solutions that we have investigated, all of the changes in morphology have been induced by adding PEG. Consequently, because PEG is inert, we attribute the changes
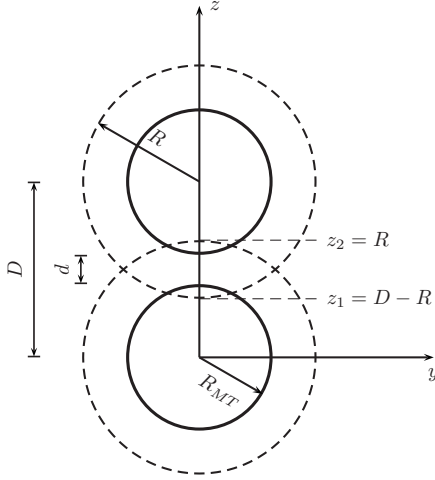
FIG. 6. Schematics showing the overlapped region of the excluded volume between two parallel MTs. The first MT is sitting along the $x$ axis and the second is translated by a distance of $D$ in the $z$ direction. The solid circles represent MTs and the dashed circles represent the depletion layers around the MTs. $d$ is the minimum surface-to-surface distance between the two MTs. $R=R_{MT}+R_{AO}$ is the total radius of the MT plus the excluded layer.

to osmotic pressure effects. In the first-order approximation of the Asakura-Oosawa (AO) model [3], the binding energy between two neighboring MTs due to the osmotic effect caused by PEG can be written as

$$\Delta E \approx P\Delta V,$$

where $P$ is the osmotic pressure and $\Delta V$ is the change of the excluded volume surrounding the two MTs. We can calculate the excluded or depletion volume associated with each MT by treating it as a cylinder with radius $R_{MT} \approx 12$ nm surrounded by a depletion layer (Fig. 6) of thickness $R_{AO} = 2R_g/\sqrt{\pi} \approx 12.9$ nm where $R_g$ is the radius of gyration of 35 kDa PEG (assuming an ideal random chain for the PEG) [39]. As two MTs approach one another their excluded volumes overlap and thus increase the accessible volume for PEG. To calculate this $\Delta V$, suppose the first MT sits along the $x$ axis and the second is translated by a distance of $D$ in the $z$ direction and rotated by an angle of $\theta$ about the $z$ axis (see Fig. 6 for an illustration in the simplest case of $\theta=0$). Setting $R$ as the total radius of the MT plus the excluded layer, $R=R_{MT}+R_{AO}$. In a Cartesian coordinate system, the equations representing the two "depletion cylinders" are as follows:

$$z^2 + y^2 \leq R^2,$$

$$(z-D)^2 + (y\cos\theta - x\sin\theta)^2 \leq R^2. \quad (1)$$

The excluded volume between these two MTs is

$$\Delta V = \int_{z_1}^{z_2} dz \int_{y_1}^{y_2} dy \int_{x_1}^{x_2} dx,$$

where $\{z_1,z_2\}$, $\{y_1,y_1\}$, and $\{x_1,x_2\}$ are integration ranges of the overlapped region between the two "depletion cylinders." From Fig. 6, we know

$$z_1 = D - R,$$

$$z_2 = R.$$

Solving Eq. (1), we obtain

$$y_1 = -\sqrt{R^2 - z^2} \leq y \leq \sqrt{R^2 - z^2} = y_2,$$

$$x_1 = \frac{1}{\sin\theta}[y\cos\theta - \sqrt{R^2 - (z-D)^2}]$$

$$\leq x \leq \frac{1}{\sin\theta}[y\cos\theta + \sqrt{R^2 - (z-D)^2}] = x_2.$$

The intersection of the depletion volume is, after the three-dimensional integration

$$\Delta V = C(\xi)\frac{(R_{MT} + R_{AO})^3}{\sin\theta}.$$

In the above equation, $C(\xi)=4\int_{\xi-1}^{1}dt\sqrt{1-(t-\xi)^2}\sqrt{1-t^2}$, where $\xi=\frac{D}{R_{MT}+R_{AO}}=\frac{d+2R_{MT}}{R_{MT}+R_{AO}}$ and $d$ is the minimum surface-to-surface distance between the two MTs. The above equation is valid as long as the overlapping excluded volume region does not reach the ends of the MTs involved. Corrections to the above equation due to the end geometry are needed only at very small $\theta$ ($\sim 2.7°$ for 0.5 $\mu$m long MTs, for instance).

Both PEG and free tubulin dimers can contribute to the osmotic pressure and thus, the osmotic binding energy. Within an ideal gas model (PEG molecules begin to overlap with each other at w/w concentration of 0.9% [5]), we can estimate the relative strength of the contribution to the osmotic pressure by PEG and tubulin dimers in our system. Assuming a 1 mg/ml critical concentration for the sample, the molar concentration of free tubulin dimers is about 10 $\mu$M. For a typical 0.5% w/w solution of 35 kDa PEG used in this study, the molar concentration of PEG is about 143 $\mu$M based on its molecular weight. Since the osmotic pressure is proportional to the molar concentration, we can conclude that the osmotic pressure generated by tubulin dimers is much smaller compared to the one generated by PEG, which gives rise to the dominant effect.

The osmotic pressure generated by the 35 kDa PEG in a 0.1% w/w solution is estimated to be $P \approx 100$ Pa [40]. In the case of two MTs in contact ($d=0$), this pressure corresponds to a binding energy $\Delta E \approx P\Delta V$, which reaches about $1k_BT$ at $\theta=45°$. Thus MTs that cross have a high probability of maintaining contact. In the case of $\theta=0°$, the binding energy per unit length between two MTs that are in contact with one another is much higher, approximately $25k_BT/\mu$m.

The osmotic torque between two crossing MTs can be obtained by differentiating $\Delta E$ with respect to $\theta$,

$$\tau_{osmotic} = PC(\xi)\frac{(R_{MT} + R_{AO})^3 \cos\theta}{\sin^2\theta}.$$

This osmotic torque exceeds the magnetic torque that is employed to initially align the samples. At $C_{PEG}$ of 0.5% and for $\theta=45°$, for instance, $\tau_{osmotic} \approx 32$ pN nm. The magnetic torque on a single MT with length $l$ is $\tau_{magnetic} \sim \Delta\chi lB^2 \sin 2\phi$ [27,31], where $B$ is the strength of the mag-
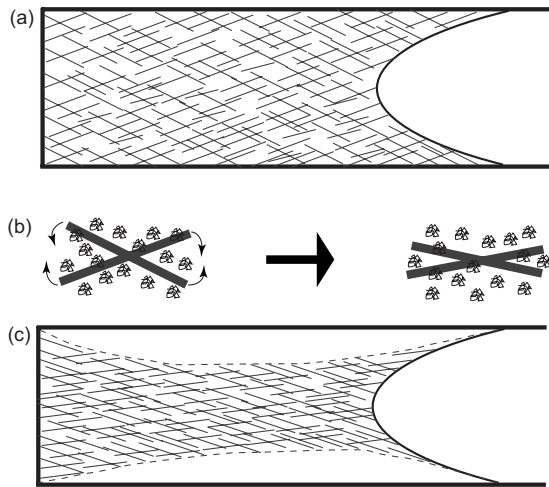
FIG. 7. Schematics (not to scale) showing the contraction of the sample due to the osmotic torque generated by PEG. (a) Depiction of MT network initially formed in the presence of PEG and a magnetic field. The gray line segments represent MT bundles. There is an overall alignment along the long axis of the cuvette by the static magnetic field. (b) Osmotic torque generated by PEG (represented by the packed polymer chains). (c) The contracted sample due to osmotic torque exerted by PEG.

netic field, $\Delta\chi$ is the anisotropy of the magnetic susceptibility of a MT per unit length and $\phi$ is the angle between the MT axis and the magnetic field direction. To estimate $\tau_{\text{magnetic}}$ we presume that $l$ corresponds to the length at which MTs are sterically hindered from rotating. For a 3.6 mg/ml tubulin sample in a 9 Tesla magnetic field, $l \approx 0.5$ $\mu$m [27] and the maximum magnetic torque is only about 0.3 pN nm, which is much smaller than the osmotic torque between two crossing MTs.

### B. Osmotic effect on MT pattern formation

In this section, we propose a qualitative model of how the enhancement of the depletion interactions between MTs can account for our experimental observations. Starting at the microscopic level, the calculation above suggests that the PEG induced osmotic forces cause MTs to come into contact while the torques act to align MTs in contact. Together, these effects tend to sequester individually dispersed MTs into bundles and to create more stable and distinct bundles that have discernible ends and thus, are relatively short [see Fig. 4(c)]. Moreover, we speculate that these distinct bundles form an interconnected network at high $C_{\text{PEG}}$ as depicted in Fig. 7. The osmotic forces cause crossing bundles that come into contact to remain in contact thereby creating network nodes. The reduction of the buckling amplitude with increasing $C_{\text{PEG}}$ (Figs. 2 and 3) can be attributed to both the loss of the dispersed network of MTs (Fig. 4) and the absence of long parallel arrays of bundles that traverse the sample volume (see Fig. 2 in Ref. [17], for example). Each of these is necessary for the coordinated buckling that generates the striped patterns. The fact that the wavelength does not appear to change as the amplitude decreases probably reflects the weak fourth root dependence of the buckling wavelength on

the mechanical properties of the bundles and the dispersed network [18].

The combination of the magnetic field applied early in the polymerization and the osmotic torques that tend to bring crossing bundles into alignment can account for the anisotropic contraction of the samples. The initial presence of the magnetic field induces a partial alignment of growing MTs that biases the overall alignment of the MT population. As the MTs bundle and cross with other bundles to form the network, however, their freedom to align independently along the magnetic field direction becomes restricted. The result, as depicted in Fig. 7(a), is a network of bundles that tend to align along the magnetic field direction. After removing a sample from the field, the osmotic torques continue to act to increase the mutual alignment of bundles in the network [see Fig. 7(b)]. Because of the bias in the network, increases in the mutual alignment lead to the lateral contraction of the sample [see Fig. 7(c)]. Alternatively, the bundling and contraction might be viewed as demixing or phase separation as described for rod and sphere mixtures [41,42].

The model proposed above can account for the fluorescence, retardance, and polarization imaging results. In that scenario, the PEG only affects the organization of the MTs and does not affect their degree of polymerization. The fluorescence and retardance images support this view. The average fluorescence intensities are comparable for $C_{\text{PEG}}=0$ and 0.5% [Figs. 2(b) and 2(c)], indicating that the MT densities are similar in the two samples. On the other hand, the average retardance intensity, which is proportional to the density of aligned MTs is higher for the sample with PEG [Fig. 3(c)]. In the PEG sample all of the bundles partially align along the initial field direction, while in the pure sample the large fraction of MTs in the dispersed network are randomly aligned.

The polarization images [Figs. 1(e)–1(n)] are consistent with the proposed model as well. In the initial stage, the intensity of light transmitted for the 45° polarization configuration [Fig. 1(g)] is greater than for the 0° configuration [Fig. 1(e)] as expected if the MTs have an average alignment along the cuvette axis. There is some transmitted intensity in the 0° configuration, which we attribute to the depolarizing scattering from the MT bundles. Later, the transmitted intensity increases for both orientations. The increase for the 0° orientation can be attributed to the further growth of depolarizing scattering as the sample continues to polymerize. On the other hand, the increase in the transmission for the 45° orientation can be attributed to both continued polymerization and greater alignment of bundles. Osmotic torques presumably drive the alignment and the accompanying lateral contraction (see schematic in Fig. 7) that is visible in both Figs. 1(f) and 1(h).

### C. Bundling mechanism and bundle size

Throughout we have presumed that the osmotic effects dominate MT bundling interaction. The large variation in MT bundle size distribution also supports this view. MT bundle formation can be mediated by specific MT associated proteins (MAPs) [43,44], molecular motors [45], counterions [8,46], or osmotic pressure [7,8]. Our recent study shows that

MT bundles spontaneously assemble in polymerizing tubulin solutions [17,18]. We hypothesize that the spontaneous bundling of MTs in the high tubulin concentrations is due to a combination of both electrostatic and depletion effects. Contribution of the former effect is from the existing ions in the tubulin buffer, but the latter is likely due to tubulin itself when present in sufficient concentrations [17]. Theoretically, the size of bundles induced by counterions has been predicted to be finite due to an energy barrier for new filament addition that increases with the bundle size [47,48]. In the presence of osmolytes, such as PEG in our case, a finite bundle size could be achieved by the balance between the repulsive force and the osmotic force. However, the depletion force is expected to be the dominant factor in bundling at high $C_{PEG}$ in our system. Two facts support this conclusion. First, the PEG molecules are not charged. Second, the Debye length at this solution salt concentration is an order of magnitude smaller than the range of the depletion attractions, which is comparable to the PEG radius. For the MT bundle size distribution measurement [Fig. 5(c)], a high $C_{PEG}$ (1% w/w) was used to ensure that all MTs were incorporated into bundles. The largest bundle measured among those shown in Fig. 5 contained around 280 MTs in the cross section. There is no reason to believe this is the limit of MT bundle size. As the number of MTs in a bundle increases, the average binding energy density per MT due to osmotic pressure stays roughly constant, and thus no size limitation from the os-

motic effects is expected. Indeed, the data shows no preferred bundle size or clear maximum size.

## V. CONCLUDING REMARKS

We have shown that the introduction of an inert macromolecule substantially alters the self-organization of MTs in solution. Specifically, a high concentration of PEG completely suppresses the spontaneous formation of MT birefringence patterns in polymerizing tubulin solutions. Microscopy shows that the PEG alters the bundling of MTs in a manner that inhibits the buckling of MT bundles necessary for the stripe formation. We analyzed the strength of osmotic forces and torques and assessed their effects on the MT assembly.

The hierarchical MT networks are among the most interesting structural features in living cells. Whereas myriad physical and biochemical factors are at play, the interplay between mechanical and osmotic forces and torques elucidated through this study likely facilitates the understanding of certain biological functions tubulin plays by the means of its dynamic self-assembly.

[1] A. P. Minton, J. Biol. Chem. **276**, 10577 (2001).

[2] R. J. Ellis and A. P. Minton, Nature (London) **425**, 27 (2003).

[3] S. Asakura and F. Oosawa, J. Chem. Phys. **22**, 1255 (1954).

[4] V. Bloomfield, Curr. Opin. Struct. Biol. **6**, 334 (1996).

[5] M. Hosek and J. X. Tang, Phys. Rev. E **69**, 051907 (2004).

[6] M. M. A. E. Claessens, M. Bathe, E. Frey, and A. R. Bausch, Nat. Mater. **5**, 748 (2006).

[7] D. J. Needleman, M. A. Ojeda-Lopez, U. Raviv, K. Ewert, J. B. Jones, H. P. Miller, L. Wilson, and C. R. Safinya, Phys. Rev. Lett. **93**, 198104 (2004).

[8] D. J. Needleman, M. A. Ojeda-Lopez, U. Raviv, K. Ewert, H. P. Miller, L. Wilson, and C. R. Safinya, Biophys. J. **89**, 3410 (2005).

[9] A. Desai and T. J. Mitchison, Annu. Rev. Cell Dev. Biol. **13**, 83 (1997).

[10] D. Bray, *Cell Movement: From Molecules to Motility* (Garland, New York, 2001).

[11] R. P. Elinson and B. Rowning, Dev. Biol. **128**, 185 (1988).

[12] G. Callaini, Development **107**, 35 (1989).

[13] F. J. Nédélec, T. Surrey, A. C. Maggs, and S. Leibler, Nature (London) **389**, 305 (1997).

[14] C. E. Walczak, I. Vernos, T. J. Mitchison, E. Karsenti, and R. Heald, Curr. Biol. **8**, 903 (1998).

[15] A. L. Hitt, A. R. Cross, and R. C. Williams, J. Biol. Chem. **265**, 1639 (1990).

[16] J. Tabony, Science **264**, 245 (1994).

[17] Y. Liu, Y. Guo, J. M. Valles, and J. Tang, Proc. Natl. Acad. Sci. U.S.A. **103**, 10654 (2006).

[18] Y. Guo, Y. Liu, J. X. Tang, and J. M. Valles, Phys. Rev. Lett. **98**, 198103 (2007).

[19] A. Suzuki, M. Yamazaki, and T. Ito, Biochemistry **28**, 6513 (1989).

[20] V. A. Parsegian, R. P. Rand, and D. C. Rau, Proc. Natl. Acad. Sci. U.S.A. **97**, 3987 (2000).

[21] N. Y. Sidorova and D. C. Rau, Proc. Natl. Acad. Sci. U.S.A. **93**, 12272 (1996).

[22] J. S. Castro, P. A. Deymier, S. D. Smith, and J. B. Hoying, Adv. Mater. (Weinheim, Ger.) **20**, 183 (2008).

[23] R. B. Vallee, Methods Enzymol. **134**, 89 (1986).

[24] W. A. Voter and H. P. Erickson, J. Biol. Chem. **259**, 430 (1984).

[25] D. L. Worcester, Proc. Natl. Acad. Sci. U.S.A. **75**, 5475 (1978).

[26] J. Torbet, J. M. Freyssinet, and G. Hudry-Clergeon, Nature (London) **289**, 91 (1981).

[27] W. Bras, G. P. Diakun, J. F. Díaz, G. Maret, H. Kramer, J. Bordas, and F. J. Medrano, Biophys. J. **74**, 1509 (1998).

[28] J. M. Denegre, J. M. Valles, K. Lin, W. B. Jordan, and K. L. Mowry, Proc. Natl. Acad. Sci. U.S.A. **95**, 14729 (1998).

[29] N. Dubey, P. C. Letourneau, and R. T. Tranquillo, Exp. Neurol. **158**, 338 (1999).

[30] N. Glade and J. Tabony, Biophys. Chem. **115**, 29 (2005).

[31] K. Guevorkian and J. M. Valles, Biophys. J. **90**, 3004 (2006).

[32] R. Oldenbourg and G. Mei, J. Microsc. **180**, 140 (1995).

[33] R. Oldenbourg, E. D. Salmon, and P. T. Tran, Biophys. J. **74**, 645 (1998).

[34] The sample was polymerized from a 3.6 mg/ml tubulin solution (2 mM GTP, 2 $\mu$M Oregon Green conjugated taxol, 100 mM PIPES, 1 mM EGTA, 2 mM MgSO$_4$, $p$H 6.9) in a $40 \times 8 \times 0.4$ mm$^3$, glass cuvette which was exposed to 9 T vertical static magnetic field for 5 min at 37 °C (the magnetic field direction is along the long axis of the cuvette). The cuvette was then laid flat on the microscope stage or between crossed polarizers for measurement at 30 °C.

[35] C. P. Brangwynne, F. C. MacKintosh, S. Kumar, N. A. Geisse, J. Talbot, L. Mahadevan, K. K. Parker, D. E. Ingber, and D. A. Weitz, J. Cell Biol. **173**, 733 (2006).

[36] J. R. LaFountain and R. Oldenbourg, Mol. Biol. Cell **15**, 5346 (2004).

[37] The sample was polymerized from a 3.6 mg/ml tubulin solution (2 mM GTP, 2 $\mu$M Oregon Green conjugated taxol, 100 mM PIPES, 1 mM EGTA, 2 mM MgS$O_4$, $p$H 6.9) in an Eppendorf tube which was incubated for 30 minutes at 37 °C. Then the sample was applied between a coverslip and a glass slide for measurement.

[38] W. Herzog and K. Weber, Eur. J. Biochem. **91**, 249 (1978).

[39] A. A. Louis, P. G. Bolhuis, E. J. Meijer, and J. P. Hansen, J. Chem. Phys. **117**, 1893 (2002).

[40] J. A. Cohen and S. Highsmith, Biophys. J. **73**, 1689 (1997).

[41] P. Bolhuis and D. Frenkel, Phys. Rev. Lett. **72**, 2211 (1994).

[42] P. Bolhuis and D. Frenkel, J. Chem. Phys. **101**, 9869 (1994).

[43] G. Lee and R. Brandt, Trends Cell Biol. **2**, 286 (1992).

[44] D. F. Albertini, B. Herman, and P. Sherline, Eur. J. Cell Biol. **33**, 134 (1984).

[45] D. Karpeev, I. S. Aranson, L. S. Tsimring, and H. G. Kaper, Phys. Rev. E **76**, 051905 (2007).

[46] J. Tang, S. Wong, P. Tran, and P. Janmey, Ber. Bunsenges. Phys. Chem. **100**, 796 (1996).

[47] B. Y. Ha and A. J. Liu, Europhys. Lett. **46**, 624 (1999).

[48] M. L. Henle and P. A. Pincus, Phys. Rev. E **71**, 060801(R) (2005).